# Investigating the $^{109}$Ag( $p$, $\gamma$) $^{110}$Cd reaction and its underlying nuclear physics

F. Heim,[1,*] J. Mayer,[1] M. Müller,[1] P. Scholz,[1,2] and A. Zilges[1]
[1]*University of Cologne, Institute for Nuclear Physics, 50937 Köln, Germany*
[2]*Department of Physics, University of Notre Dame, Indiana 46556-5670, USA*

(Received 10 March 2021; accepted 29 April 2021; published 10 May 2021)

**Background:** The nucleosynthesis of neutron-deficient $p$ nuclei remains an unsolved puzzle in nuclear astrophysics. Most likely, huge networks containing hundreds of nuclear reactions are responsible for the creation of this group of nuclei. In reality, many of the relevant reaction rates cannot be studied experimentally but need to be estimated using global and robust theoretical approaches. The underlying nuclear physics that enters these calculations is often still not constrained well enough, especially for nuclei further off the valley of stability.
**Purpose:** Here, we complete the systematic measurement of radiative proton-capture reactions on stable Ag isotopes. The results will be used to test existing theoretical models and are crucial to constrain underlying nuclear physics properties. For this purpose, total cross sections of the $^{109}$Ag($p$, $\gamma$) $^{110}$Cd reaction have been measured at proton energies between 2.5 and 5.0 MeV.
**Method:** The cross-section measurements have been carried out by means of in-beam $\gamma$-ray spectroscopy and the observation of all ground-state transitions in $^{110}$Cd. In general, the total cross sections depend strongly on the $\gamma$-ray strength function ($\gamma$-SF) and the nuclear level density (NLD). While the former one is taken from the systematics in other even-even Cd isotopes, the NLD has been constrained by renormalizing microscopic, tabulated values onto the low-lying cumulative number of levels.
**Results:** For the first time, $^{109}$Ag($p$, $\gamma$) $^{110}$Cd reaction cross sections have been reported over a wide range of beam energies. The total cross-section results are in good agreement with a rather limited, formerly published dataset. A convincing agreement with recent Hauser-Feshbach calculations is received when using existing descriptions for the $\gamma$-SF and a renormalized, microscopic NLD model.
**Conclusion:** The measured cross sections confirmed the reliability of existing theoretical models used in Hauser-Feshbach statistical model calculations. Coherent results are obtained for the statistical nuclear physics properties in the even-even Cd isotopes as well as for the derived experimental cross sections.

DOI: 10.1103/PhysRevC.103.055803

## I. INTRODUCTION

For more than 60 years we know that the majority of heavy nuclei beyond the iron peak is created by neutron capture processes [1–4]. However, a group of 30 to 35 stable, proton-rich nuclei ranging from $^{74}$Se to $^{196}$Hg is bypassed by these processes [5–7]. The different mechanisms that trigger the nucleosynthesis of these $p$ nuclei are commonly denoted as $p$ processes. Investigation of the astrophysical sites as well as the impact of nuclear physics within the $p$ processes is going on for about four decades and still leaves us with many open questions.

Among the various processes that are considered to be responsible for $p$-process nucleosynthesis (see, e.g., Ref. [6]) the largest contribution is expected from photodisintegration reactions on stable $s$- or $r$-process seed nuclei, the so-called $\gamma$ process [6,8,9].

To understand the details of the $\gamma$ process the interplay of astronomy, astrophysics and nuclear physics is of great importance. From an astrophysical point of view the exact scenario and its conditions need to be constrained. For many years, SNII explosions have been the best candidate [8,9]. However, additional $p$-process contributions have been found in supernova type Ia [10], but a more thorough analysis of the role of SNe Ia in the solar composition of $p$ nuclei is needed [11,12]. From a nuclear physics point of view, the photodisintegration rates which are acting in the complex $\gamma$ process network play an important role, which are most heavily governed by the intrinsic nuclear physics properties of the involved nuclei. Obviously, not all reaction rates comprised in this network can be accessed experimentally at astrophysically relevant conditions, in particular when unstable nuclei are involved. Consequently, reliable theoretical models have to be employed to predict the respective cross sections or to extrapolate them to astrophysical energies, i.e., far below the Coulomb barrier [13,14]. Therefore, it is essential to test the calculated cross sections experimentally in accessible energy ranges and to provide more robust input to the network calculations and improve their predictive power.

Theoretical cross sections and reaction rates are usually obtained using the Hauser-Feshbach statistical model [15,16], and the results are mainly affected by the nuclear physics input parameters such as $\gamma$-ray strength functions ($\gamma$-SF), nuclear

*fheim@ikp.uni-koeln.de

 

level densities (NLD), and particle + nucleus optical-model potentials (OMPs) [5,17]. In radiative capture reactions, the $\gamma$-SF and NLD showed to have the most significant impact on the calculated cross-section results at astrophysical energies [5,6,17]. According to the latest experimental reports, it was found that the established proton and neutron optical-model potentials provide very accurate results, whereas the available $\alpha$-OMPs can easily yield discrepancies between experimental and calculated cross sections of a factor of three or even more (see, e.g., Refs. [18–24] and references therein).

Previously, we performed radiative proton capture studies on $^{107}$Ag [25], the only other stable nucleus in the silver chain. The measured cross sections have been used to study the statistical $\gamma$-decay behavior in the compound nucleus $^{108}$Cd. The derived data for the $\gamma$-SF as well as for the NLD in the $p$ nucleus $^{108}$Cd are in great agreement with the systematics found in the other even-even isotopes $^{106,112}$Cd. Hence, the aim of this work is to complete the experimental database for proton-capture reactions on stable Ag isotopes by measuring the $^{109}$Ag$(p,\gamma)^{110}$Cd cross section, for which only one minor experimental dataset is available [26].

Although the $^{109}$Ag$(p,\gamma)^{110}$Cd reaction is not of direct astrophysical relevance, its results are very valuable to test the accuracy of Hauser-Feshbach statistical model calculations. In particular, the nucleosynthesis of several $p$ nuclei in the Cd-Sn-In region is quite complex [27,28] and reliable cross-section calculations for the $\gamma$-process network in this mass region are necessary, see, e.g., Refs. [29,30]. For that reason, the total cross sections obtained in this work are compared with statistical model calculations using the TALYS [31] code in version 1.95 aiming at a systematic investigation of the respective nuclear-physics models entering the calculations, namely, the nuclear level density and the $\gamma$-ray strength function in $^{110}$Cd. Finally, we compare NLD and $\gamma$-SF data for $^{110}$Cd to experimental and theoretical data for the neighboring even-even Cd isotopes.

This paper is structured as follows: In Sec. II a brief summary of the experimental setup and method is given, followed by an overview of the data analysis in Sec. III. In Sec. IV our experimental results are presented and the statistical model analysis using TALYS [31] is discussed.

## II. EXPERIMENTAL SETUP AND METHOD

The analysis of the $^{109}$Ag$(p,\gamma)^{110}$Cd reaction has been carried out by means of high-resolution in-beam $\gamma$-ray spectroscopy. This method has been described, e.g., in Refs. [21,25,33–39] and is feasible for all reactions involving a stable target nucleus. The reaction product, however can be either stable or unstable. The irradiation has been performed at the 10 MV FN-Tandem accelerator at the Institute for Nuclear Physics at the University of Cologne. After the proton capture, an excited compound nucleus is formed which subsequently deexcites into low-lying levels via $\gamma$-ray emission. The excitation energy $E_x$ is given by

$$E_x = Q + E_{\mathrm{c.m.}}, \tag{1}$$

where $Q$ denotes the $Q$ value of 8917 keV for the $^{109}$Ag$(p,\gamma)^{110}$Cd reaction and $E_{c.m}$ denotes the center-of-mass energy. Finally, all reaction products will reach its respective ground state, hence by observing all ground-state transitions the total number of produced compound nuclei can be derived. The reaction scheme is illustrated in Fig. 1. The respective $\gamma$ rays have been detected using the HORUS $\gamma$-ray spectrometer which holds 14 HPGe detectors. The experimental setup as well as details about the in-beam $\gamma$-ray spectroscopy method for nuclear astrophysics is described in Ref. [38].

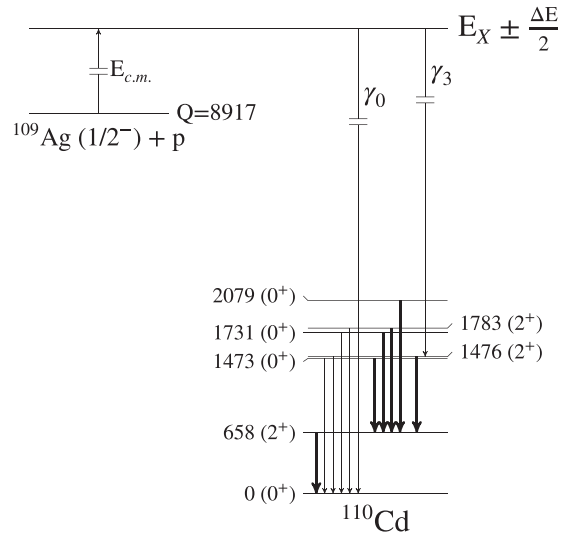


FIG. 1. Schematic illustration of the radiative proton-capture reaction on $^{109}$Ag. The formed compound state contains numerous unresolvable resonances and has a width of $\frac{\Delta E}{2}$, where $\Delta$E denotes the energy loss. It then deexcites either directly into the ground state of $^{110}$Cd ($\gamma_0$) or into other low-lying levels via different $\gamma$-ray cascades. Only states which can deexcite at least partly into the ground state are shown. The dominant branchings are shown by thick arrows. All data are taken from Ref. [32].

As also depicted in Fig. 1, the prompt $\gamma$-ray decay into different discrete states in $^{110}$Cd can be observed, which allows us to calculate partial cross sections. These transitions are denoted as $\gamma_x$, where $x$ stands for the respective populated state ($x = 0, 1, 2, ...$).

Generally, absolute cross sections are given by

$$\sigma(p,\gamma)_{\mathrm{tot}} = \frac{N_{(p,\gamma)}}{N_P N_T}, \tag{2}$$

where $N_P$ and $N_T$ are the number of projectiles and target nuclei per area, respectively, and $N_{(p,\gamma)}$ is the number of proton-capture reactions which is derived from the $\gamma$-ray spectra. After creation of the excited compound nucleus, each emitted $\gamma$ ray follows an angular distribution $W(\Theta)$ with respect to the beam axis. The experimental yield $Y(E_\gamma)$ is corrected for the full-energy peak efficiency $\epsilon(E_\gamma)$ and the dead time of the data acquisition $\tau$:

$$W(\Theta) = \frac{Y(E_\gamma)}{\epsilon(E_\gamma)\tau}. \tag{3}$$

The angular distribution is obtained by fitting a sum of Legendre polynomials to the experimental values:

$$W(\Theta) = A_0\left(1 + \sum_{k=2,4} \alpha_k P_k(\cos\Theta)\right) \quad (4)$$

These angular distributions are obtained for each $\gamma$-ray transition at each beam energy and the sum of all $A_0$ coefficients represents the total number of proton captures, $N_{(p,\gamma)}$ [38].

## III. DATA ANALYSIS

### A. Particle beam details

Proton beams with energies between $E_p = 2.5$ MeV and $E_p = 5.0$ MeV have been chosen to ensure that the astrophysical relevant Gamow window for the $^{109}$Ag$(p,\gamma)$ $^{110}$Cd reaction, which lies between 2.02 and 4.25 MeV at $T = 3.0$ GK, is approximately covered in this experiment. Beam intensity and the duration of measurement varied with the beam energy as the reaction cross sections are expected to decrease with decreasing beam energy. For the highest proton energies, data were recorded for 1–2 hours at beam currents of about 300 nA, whereas for the lowest energy of $E_p = 2500$ keV the intensity was increased to about 610 nA for 24 hours. Additionally, a 94 hour, long-term measurement with beam currents of about 820 nA was performed using 4.0 MeV protons to study the reaction of interest in great detail. In particular, this measurement was used to estimate the relative intensity of various ground-state transitions that are used to calculate the total cross section. These information can be used later for all measurements where only the strongest $\gamma$-ray transitions can be observed (see Sec. III C).

### B. Target properties

Two highly enriched (99%) $^{109}$Ag targets of 1.14(11) and 1.38(14) mg/cm$^2$ thickness have been manufactured at the in-house target laboratory as self-supporting foils via rolling. During irradiation, a 200-mg/cm$^2$-thick gold foil was attached to the backside of the targets to stop the beam reducing the beam-induced background at material at the down-beam end of the target chamber. The target thickness was determined using Rutherford backscattering spectrometry (RBS) at the RUBION facility in Bochum, Germany before the experiment as well as during the experiment using the RBS detector mounted at the target chamber in Cologne [25,38]. The respective energy loss $\Delta E$ inside the target was simulated using the SRIM [40] code, and amounted on average to 41 to 63 keV, depending on the beam energy. The effective interaction energy of the protons is defined as

$$E_{\text{eff}} = E_p - \frac{\Delta E}{2}, \quad (5)$$

where $E_p$ denotes the beam energy of the impinging protons.

Unfortunately, it was observed that a significant amount of target material was deteriorated during the last measurement using the 3.0 MeV proton beam. To determine the effective target thickness during the irradiation, the intensity of the 311 keV $\gamma$-ray transition in $^{109}$Ag stemming from Coulomb excitation was normalized to the 279 keV $\gamma$-ray transition in the $^{197}$Au backing in time steps of ten minutes, see Fig. 2. Apparently, at the beginning of the irradiation a large amount of material seems to be deteriorated but after some time the target composition remains stable and constant. Hence, for the analysis of this measurement only data recorded after the deterioration were taken into account, i.e., when the target thickness stayed constant. Since the deterioration process started right after the beginning of irradiation, the initial 311–279 keV ratio for the beam energy of $E_p = 3.0$ MeV is not known and, therefore, the absolute target thickness after deterioration is unclear. However, the 311–279 keV ratio depends on the respective cross sections for Coulomb excitation and is expected to follow a smooth trend as a function of beam energy. Figure 3 shows the 311–279 keV ratio for each beam energy used in this experiment. An analytical function of the

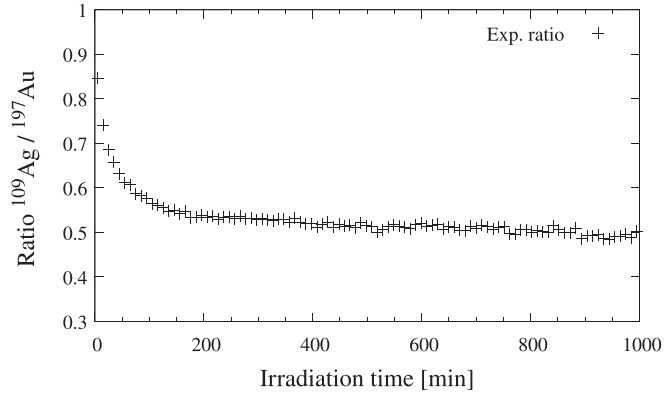


FIG. 2. Experimental 311-to-279 keV peak volume ratio as a function of irradiation time for the $E_p = 3.0$ MeV measurement. The 311 and 279 keV $\gamma$ rays stem from Coulomb excitation on $^{109}$Ag (target) and $^{197}$Au (backing), respectively. Each data point represents a measured time interval of 10 minutes. Right at the beginning of the irradiation a significant amount of target material has been deteriorated. The error bars are too small to be visible.

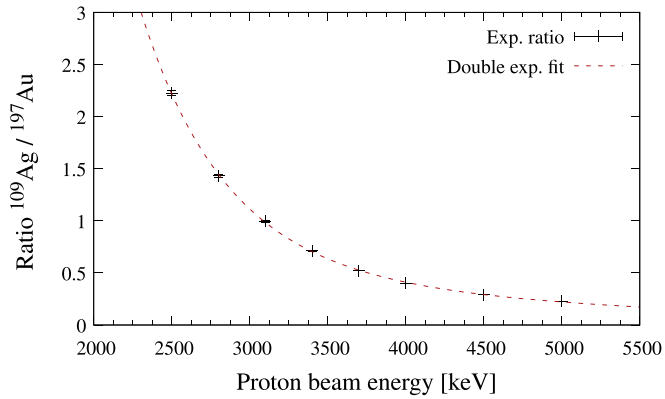


FIG. 3. Experimental 311-to-279 keV peak volume ratio shown as a function of proton beam energy. For a target of constant thickness, the ratio depends only on the beam energy. A double exponential fit function has been employed to interpolate the initial ratio for a beam energy of $E_p = 3.0$ MeV (see Fig. 2).

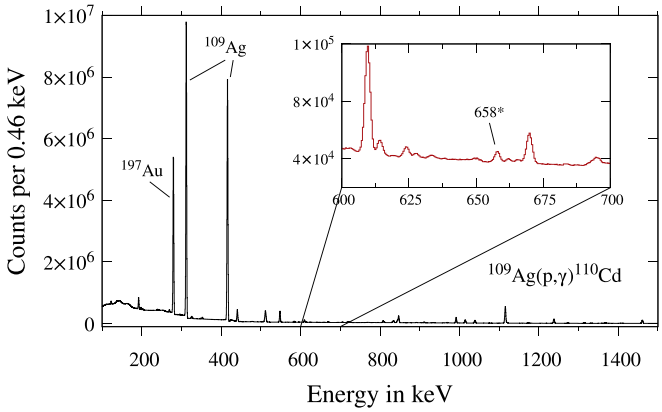


FIG. 4. Excerpt from a spectrum of the $^{109}$Ag$(p,\gamma)^{110}$Cd reaction for a proton beam of $E_p = 2.5$ MeV. The data shown in the spectrum have been recorded for about 24 hours from 14 HPGe detectors. As one can see, the spectrum is dominated by Coulomb excitation on the target and stopper material. The $2_1^+ \rightarrow$ g.s. transition at $E_\gamma = 658$ keV is marked with an asterisk.

form

$$f(x) = ae^{bx} + ce^{dx} \tag{6}$$

has been fit to the values to interpolate the initial ratio for the beam energy of 3.0 MeV. Note that we accounted for the different thicknesses of the used targets for each respective beam energy in Fig. 3.

### C. $\gamma$-ray detection

The $\gamma$ rays emitted after the $^{109}$Ag$(p,\gamma)^{110}$Cd reaction have been detected by the 14 HPGe detectors which are mounted at five different angles with respect to the beam axis inside the HORUS $\gamma$-ray spectrometer [38]. Absolute efficiencies for $\gamma$-ray energies up to 2 MeV were determined using a $^{226}$Ra standard calibration source. For absolute $\gamma$-ray detection efficiencies of $\gamma$-ray energies up to 5 MeV, in-house-produced $^{56}$Co and $^{66}$Ga sources have been used. These sources have half-lives of 77 days and 9.5 hours, respectively, but emit numerous $\gamma$ rays up to an energy of $E_\gamma = 4.8$ MeV [41,42]. The total detection efficiency of the HORUS array amounts to about 3% at $E_\gamma = 1.3$ MeV in the configuration used for this experiment.

Using high-resolution in-beam $\gamma$-ray spectroscopy, total cross sections can be derived by summing up the yield of all ground-state (g.s.) transitions. The experimental yield $Y(E_\gamma)$ for each ground-state transition in $^{110}$Cd is obtained from the $\gamma$-ray spectra. A typical $\gamma$-ray spectrum for the beam energy of $E_p = 2.5$ MeV is shown in Fig. 4. The main plot shows the $\gamma$-ray spectrum over a wide energy range which is dominated by Coulomb excitation in the target material and the gold backing. The inset shows the energy region around the strongest ground-state transition in $^{110}$Cd with an energy of $E_\gamma = 658$ keV. The spectrum was obtained after 24 hours of recording at an average beam intensity of 610 nA. All other peaks that were found either stem from reactions on the stable copper isotopes $^{63,65}$Cu inside the cooling tube that surrounds the target or from the $^{109}$Ag$(p,n)^{109}$Cd reaction.

TABLE I. Total cross-section values $\sigma_{\text{tot}}$ for the $^{109}$Ag$(p,\gamma)^{110}$Cd reaction as a function of center-of-mass beam energy corrected for the energy loss within the target. See text for details.

| $E_{\text{c.m.}}$ [keV] | $\sigma_{\text{tot}}$ [$\mu$b] |
|---|---|
| 2446 ± 26 | 0.48 ± 0.06 |
| 2775 ± 26 | 1.69 ± 0.19 |
| 2944 ± 26 | 2.80 ± 0.32 |
| 3044 ± 26 | 3.89 ± 0.45 |
| 3343 ± 26 | 7.81 ± 0.91 |
| 3642 ± 26 | 15.4 ± 1.8 |
| 3941 ± 26 | 31.7 ± 1.9 |
| 4437 ± 26 | 60.9 ± 7.0 |
| 4935 ± 26 | 97.8 ± 11.2 |

Experimentally, barely any significant contribution from other g.s. transitions apart from the $E_\gamma = 658$ keV transition has been found in the singles $\gamma$-ray spectra. The only other g.s. transition with a non-negligible peak volume originates from the $2_2^+$ state at $E_x = 1476$ keV. Its intensity amounts to about 5% compared with the $E_\gamma = 658$ keV transition. As explained earlier, a long-term measurement at high beam intensities was used to estimate the impact of other ground-state transitions in $^{110}$Cd. Figure 1 shows the low-lying levels in $^{110}$Cd and their strongest $\gamma$-ray transitions. All states that can decay into the g.s. exhibit a dominating $\gamma$-decay branching into the $2_1^+$ state at $E_\gamma = 658$ keV. To estimate the intensity of other g.s. transitions, we applied the $\gamma\gamma$-coincidence technique [25,38,39,43]. Via setting a gate on the $E_\gamma = 658$ keV transition, all states that branch into the $2_1^+$ state become visible. With this very sensitive method, other g.s. transitions have been identified but their overall contribution to the total g.s. population amounts to less than 1% and have been neglected during the analysis. In summary, it turned out, that after the proton capture the excited $^{110}$Cd nucleus transitions into its ground state via the $2_1^+$ state in about 95% of all cases. The remaining 5% of the g.s. population proceeds via the $2_2^+$ state at $E_x = 1476$ keV. Also, no prompt $\gamma$ decay ($\gamma_0$) from the excited compound nucleus into the g.s. was observed.

## IV. RESULTS AND ANALYSIS

### A. Total cross-section results

The total cross-section values obtained in this work are listed in Table I. Energies are given as effective center-of-mass energies corrected for the energy loss. The uncertainties in the cross section values are composed of the uncertainties in the number of projectiles (≈5%), the target thickness (≈10%), full-energy peak efficiency (≈4%), and the statistical error after fitting the Legendre polynomials (≈3%).

For the $^{109}$Ag$(p,\gamma)^{110}$Cd reaction previously measured, data have been published by Khaliel *et al.* [26]. However, the reported measurements provided only three data points with very high relative uncertainties of up to 400%. Figure 5 shows the cross-section values obtained in the present work along with the data reported in Ref. [26]. Within the uncertainty ranges, a good agreement between the data sets is given.

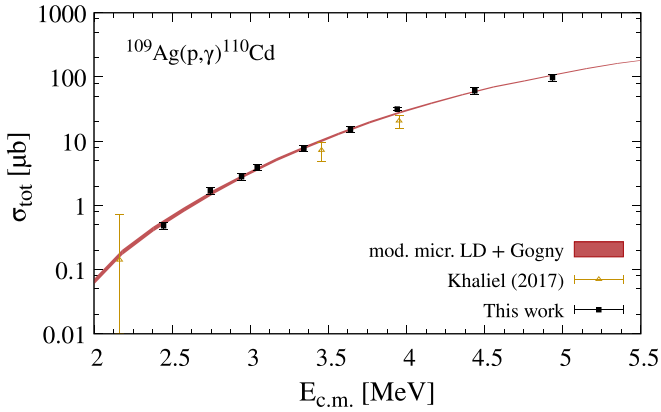


FIG. 5. Experimental total $^{109}$Ag$(p,\gamma)$ $^{110}$Cd cross sections obtained in this work (black squares) and reported in Ref. [26] (yellow triangles). Statistical model calculations using the TALYS 1.95 code [31] have been performed. The microscopic level densities from Hilaire's combinatorial tables [44] have been renormalized, as explained in Sec. IV C. For the $\gamma$-SF the Gogny D1M + QRPA model has been used [45]. The narrow, red shaded area depicts the range of calculated cross sections by including the zero-limit extension of the Gogny D1M + QRPA strength function model [46].

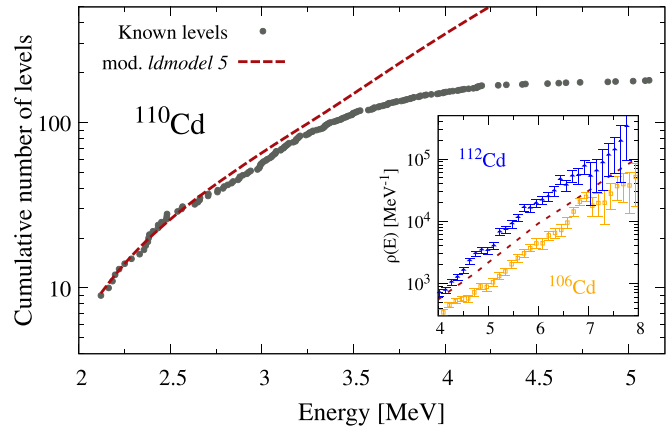


FIG. 6. (main window) Cumulative number of levels in $^{110}$Cd reported in Ref. [32] (gray circles). In addition, the renormalized microscopic level densities from Hilaire's tables in Ref. [44] are shown as *modified ldmodel5*. The same parametrization has been used as input for the TALYS calculations. See Sec. IV C for details. (small window) Experimental level densities for two other isotopes, $^{106,112}$Cd from Ref. [56] at high energies are consistent with the level-density model employed in this work.

### B. Statistical model analysis

The reliability of calculated cross sections using a Hauser-Feshbach code like TALYS is mainly governed by the models chosen for the nuclear-physics input parameters. In the case of $(p,\gamma)$ reactions, the most important parameters are the nuclear level density (NLD), $\gamma$-ray strength function ($\gamma$-SF), and particle + nucleus OMPs. Proton and neutron OMP have been thoroughly investigated via nucleon-scattering experiments for over 50 years, see, e.g., [47,48], and global models like the Koning and Delaroche OMP [49] have proven their reliability and robustness. Therefore, we will focus on the impact of NLD and $\gamma$-SF in the following. However, in contrast with the simple concept of comparing theoretical results using all available models for NLD and $\gamma$-SF to experimental values, we presented a more strategical and systematical approach in another recent work [25,39]: From the numerous models and parametrizations that are available for the NLD, we will search for the best reproduction of the experimentally determined cumulative number of low-lying levels in $^{110}$Cd. The systematic behavior of the level density in the even-even Cd isotopes is additionally studied by looking at measured level densities using the Oslo method, see, e.g., Ref. [50]. The $\gamma$-SF in the Cd isotopes has also been investigated experimentally in the past and follows a very equal pattern in all isotopes. In the end, all of these information are used to obtain a coherent set of nuclear physics models for the Cd isotopes and will be used as input for the statistical model calculations.

### C. Level-density studies

Theoretical NLD models are used to calculate the number of levels and the spin-parity distribution at a certain excitation energy. Especially at higher energies, the level spacing becomes very small and levels cannot be counted individually [51]. In the last years microscopic NLD models based on a combinatorial approach have shown their predictive power [44,52] and by now, they can be tuned to the same level of accuracy as phenomenological models like the back-shifted Fermi gas model [53] or the Gilbert-Cameron Model [54]. Moreover, the spin and parity distributions are based on a more realistic combinatorial approach. In many cases, an equal-parity assumption is not able to reproduce experimental findings, see, e.g., Ref. [55]. Similar to our analysis in Refs. [25,39], for $^{110}$Cd we choose to start with Hilaire's tabulated, microscopic level densities based on Hartree-Fock-Bogoliubov (HFB) calculations and the Skyrme interaction [44]. In TALYS this is implemented as *ldmodel 5*.

The tabulated, microscopic level-density values $\rho_{\rm tab}$ are composed of the level densities for positive and negative parity and can be adjusted within the TALYS code via the following parametrization:

$$\rho(E_x, J, \pi) = e^{c\sqrt{E_x-\delta}}\rho_{\rm tab}(E_x-\delta, J, \pi), \qquad (7)$$

where by default the scaling parameter $c = 0$ and the "pairing shift" $\delta$ gives the opportunity to obtain the level density at a different energy, i.e., to shift the NLD. Please note that the opportunity to use these scaling options does not put the microscopic models automatically on the level of phenomenological ones. Usually, these parameters need to be adjusted to fit experimental results [14,44].

We varied the aforementioned scaling parameters to find the best agreement between the number of cumulative levels predicted by the NLD model and those known from experiments up to an excitation energy of 2.7 MeV. At higher energies the experimental level information becomes scarce and the level scheme might not be complete. Figure 6 shows the cumulative number of levels in $^{110}$Cd along with the predictions of the microscopic level-density model using the best set of parameters of $c = -0.18$ and $\delta = 0.48$. Naturally, the NLD models shall not only describe the low-lying number of

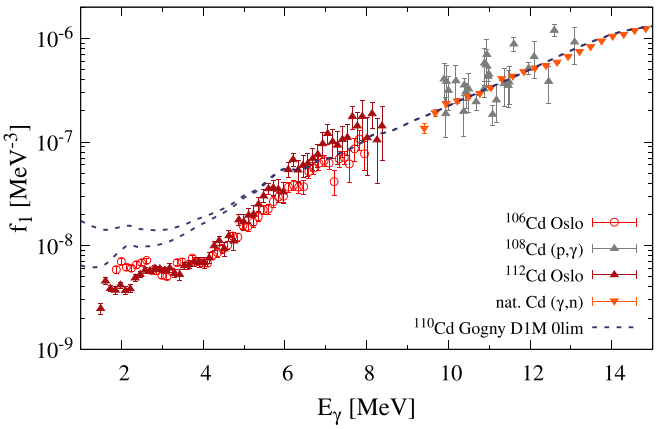


FIG. 7. Dipole components of the $\gamma$-ray strength functions in even-even Cd isotopes as sum of $E1$ and $M1$ contributions. Experimental data has been taken from Ref. [56]. Additionally, microscopic calculations of the Gogny D1M + QRPA in the zero-lim extension are shown [46].

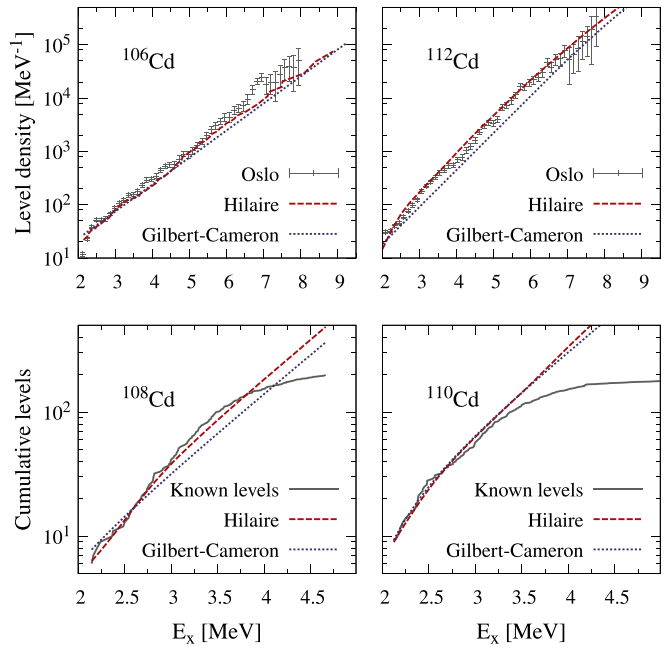


FIG. 8. Comparison of the microscopic NLD model from Ref. [44] and the Gilbert-Cameron model [54] for the even-even Cd isotopes. Where available, experimental level densities derived by means of the Oslo technique are shown [56]. For the other cases, the cumulative number of levels are used to compare the level densities. For $^{106}$Cd and $^{110}$Cd both NLD models provide fairly comparable predictions which are also in good agreement with experimental results. However, for $^{108}$Cd and $^{112}$Cd, the microscopic level-density model shows a much better agreement.

levels sufficiently, but also predicts the level density at high excitation energies accurately. For that purpose, we compared the level-density predictions in $^{110}$Cd to experimental level densities in other even-even Cd isotopes [25,56], see the inset of Fig. 6. The systematics is well-described by the adjusted NLD model and confirms the predictive power of the chosen microscopic NLD model.

### D. The $\gamma$-ray strength function taken from systematics

The $\gamma$-ray strength function in the Cd isotopes has been subject of detailed investigation and experimental data have been extracted by means of the Oslo technique a few years ago [56]. The results give a quiet coherent picture of the $\gamma$-SF in the Cd isotopes. In the last years, heavy effort has been put into large-scale calculations of theoretical $\gamma$-SF models obtained in the framework of the quasiparticle random-phase approximation (QRPA) (see, e.g., Refs. [57–59]). Calculations based on the Gogny D1M-QRPA approach [45] have shown to provide very satisfying agreement with experimental results and recently have been additionally extended to describe the nonzero limit of the $\gamma$-SF [46], which has been observed experimentally at low photon energies [60,61]. Figure 7 shows the $\gamma$-ray strength function in the even-even Cd isotopes $^{106,112}$Cd from Ref. [56] as well as photoabsorption cross sections on natural cadmium reported in Ref. [62]. In addition, we show $\gamma$-ray strength function data in $^{108}$Cd derived from radiative proton capture on $^{107}$Ag [25]. Overall, the Gogny D1M + QRPA in the zero-limit extension is in good agreement with the data extracted from the Oslo method and hence, we have chosen it for our statistical model calculations.

### E. Discussion

The experimental $^{109}$Ag$(p,\gamma)^{110}$Cd cross sections obtained in this work are shown in Fig. 5 along with statistical model calculations using the TALYS code. The models for the level-density model as well as for the $\gamma$-ray strength function have been chosen as explained in the previous sections. Overall, a very good agreement between experimental and theoretical cross sections is given. This is not too surprising because we chose the nuclear physics properties consistent with the systematics in other even-even Cd isotopes. Thus, the statistical $\gamma$-decay behavior in the even-even Cd isotopes is expected to be described sufficiently well by the employed microscopic models. It is worth mentioning that we used the Gogny D1M + QRPA strength function model with and without the zero-limit extension to calculate the total $(p,\gamma)$ cross sections. The red shaded region in Fig. 5 includes the results using both models. It appears, that the low-energy enhancement has no major impact on the calculated values.

Finally, we briefly discuss the predictive power and reliability of different NLD models by means of experimental data from the even-even Cd isotopes. As outlined earlier, the underlying nuclear physics that governs the reaction network within the $p$ process needs to be predicted by theory for many nuclei. In particular, extrapolations for nuclei far off the valley of stability are required. In Fig. 8 we illustrate the deviations between the level densities predicted by the microscopic NLD model from Ref. [44] and the commonly used constant-temperature model (CTM) by Gilbert and Cameron [54] for even-even Cd isotopes. For $^{106}$Cd and $^{112}$Cd the theoretical predictions are compared with experimental level densities obtained by means of the Oslo technique. For $^{108}$Cd and $^{110}$Cd, no experimental level densities are available,

hence we use the cumulative number of levels as benchmark. It can be observed that a reasonable agreement between experiments and predictions from the microscopic model is obtained consistently for all Cd isotopes. The Gilbert-Cameron model as it is used in the TALYS code on the other hand, fails for $^{108}$Cd and $^{112}$Cd and does not provide accurate results. This definitely supports the quality of microscopic models and demonstrates, at least in the case of the Cd isotopes, their high predictive power.

## V. SUMMARY AND CONCLUSION

In this paper, the experimental cross sections of the $^{109}$Ag$(p, \gamma)$ $^{110}$Cd reaction at proton beam energies between 2.5 and 5 MeV have been investigated. Via the radiative proton-capture on $^{109}$Ag the nuclear physics properties in $^{110}$Cd can be accessed and studied. For the statistical model analysis of the cross-section data we could disentangle the effects of NLD and $\gamma$-SF, which are crucial parameters that enter the statistical model calculations. The NLD has been fixed to the number of known levels in $^{110}$Cd with respect to the microscopic HFB level-density model from Ref. [44]. The employed level-density model has been shown to give very reliable predictions for the even-even Cd isotopes.

The recently published D1M + QRPA + 0lim $\gamma$-SF model calculations [46], which are an extension of the Gogny D1M + QRPA photoabsorption model to the deexcitation mechanism and include recent experimental findings with respect to the low-energy limit, have shown to be well suited to reproduce experimental $\gamma$-SF data. The total $^{109}$Ag$(p, \gamma)$ $^{110}$Cd cross sections can be nicely described by statistical model calculations using the aforementioned models as nuclear physics input. However, it was found that the low-energy enhancement of the $\gamma$-SF in $^{110}$Cd has no significant impact on the cross-section values, in contrast with the findings in $^{94}$Mo, where the low-energy enhancement is required [39].

Finally, the $^{109}$Ag$(p, \gamma)$ $^{110}$Cd cross-section measurement delivers further experimental constraints on the models for the underlying nuclear physics that govern nuclear reaction rates. In particular, we are searching for global and robust models which provide reliable data for nuclei that are beyond experimental reach which can most likely be realized by utilizing models that are of microscopic nature.

## ACKNOWLEDGMENTS

We gratefully thank K.O. Zell and A. Blazhev for the target preparation and H.W. Becker and V. Foteinou of the Ruhr-Universität Bochum for the assistance during the RBS measurements. This project has been supported by the Deutsche Forschungsgemeinschaft under the contract ZI 510/9-1.

[1] E. M. Burbidge, G. R. Burbidge, W. A. Fowler, and F. Hoyle, Rev. Mod. Phys. **29**, 547 (1957).
[2] F. Käppeler, R. Gallino, S. Bisterzo, and W. Aoki, Rev. Mod. Phys. **83**, 157 (2011).
[3] M. Pignatari, R. Gallino, M. Heil, M. Wiescher, F. Käppeler, F. Herwig, and S. Bisterzo, Astrophys. J. **710**, 1557 (2010).
[4] M. Arnould, S. Goriely, and K. Takahashi, Phys. Rep. **450**, 97 (2007).
[5] M. Arnould and S. Goriely, Phys. Rep. **384**, 1 (2003).
[6] T. Rauscher, N. Dauphas, I. Dillmann, C. Fröhlich, Zs. Fülöp, and Gy. Gyürky, Rep. Prog. Phys. **76**, 066201 (2013).
[7] M. Pignatari, K. Göbel, R. Reifarth, and C. Travaglio, Int. J. Mod. Phys. E **25**, 1630003 (2016).
[8] S. E. Woosley and W. M. Howard, Astrophys. J., Suppl. Ser. **36**, 285 (1978).
[9] M. Rayet, M. Arnould, M. Hashimoto, N. Prantzos, and K. Nomoto, Astron. Astrophys. **298**, 517 (1995).
[10] C. Travaglio, F. K. Röpke, R. Gallino, and W. Hillebrandt, Astrophys. J. **739**, 93 (2011).
[11] C. Travaglio, R. Gallino, T. Rauscher, F. K. Röpke, and W. Hillebrandt, Astrophys. J. Lett. **799**, 54 (2015).
[12] C. Travaglio, T. Rauscher, A. Heger, M. Pignatari, and C. West, Astrophys. J. Lett. **854**, 18 (2018).
[13] H. Schatz, J. Phys. G **43**, 064001 (2016).
[14] S. Goriely, Eur. Phys. J. A **51**, 172 (2015).
[15] W. Hauser and H. Feshbach, Phys. Rev. **87**, 366 (1952).
[16] T. Rauscher and F.-K. Thielemann, At. Data Nucl. Data Tables **75**, 1 (2000).
[17] T. Rauscher, Int. J. Mod. Phys. E **20**, 1071 (2011).
[18] G. G Kiss, P. Mohr, Zs. Fülöp, T. Rauscher, Gy. Gyürky, T. Szücs, Z. Halász, E. Somorjai, A. Ornelas, C. Yalçin, R. T. Güray, and N. Özkan, Phys. Rev. C **88**, 045804 (2013).
[19] S. J. Quinn, A. Spyrou, A. Simon *et al.*, Phys. Rev. C **92**, 045805 (2015).
[20] A. Simon, M. Beard, A. Spyrou, S. J. Quinn *et al.*, Phys. Rev. C **92**, 025806 (2015).
[21] L. Netterdon, J. Mayer, P. Scholz, and A. Zilges, Phys. Rev. C **91**, 035801 (2015).
[22] P. Scholz, F. Heim, J. Mayer, C. Münker, L. Netterdon, F. Wombacher, and A. Zilges, Phys. Lett. B **761**, 247 (2016).
[23] T. Szücs, P. Mohr, Gy. Gyürky, Z. Halász, R. Huszánk, G. G. Kiss, T. N. Szegedi, Zs. Török, and Zs. Fülöp, Phys. Rev. C **100**, 065803 (2019).
[24] P. Scholz *et al.*, Phys. Rev. C **102**, 045811 (2020).
[25] F. Heim, P. Scholz, M. Körschgen, J. Mayer, M. Müller, and A. Zilges, Phys. Rev. C **101**, 035805 (2020).
[26] A. Khaliel, T. J. Mertzimekis, E.-M. Asimakopoulou, A. Kanellakopoulos, V. Lagaki, A. Psaltis, I. Psyrra, and E. Mavrommatis, Phys. Rev. C **96**, 035806 (2017).
[27] Z. Németh, F. Käppeler, C. Theis, T. Belgya, and S. W. Yates, Astrophys. J. **426**, 357 (1994).
[28] C. Theis, F. Käppeler, K. Wisshak, and F. Voss, Astrophys. J. **500**, 1039 (1998).
[29] A. Psaltis *et al.*, Phys. Rev. C **99**, 065807 (2019).
[30] O. Olivas-Gomez, A. Simon *et al.*, Phys. Rev. C **102**, 055806 (2020).
[31] A. Koning and D. Rochman, Nucl. Data Sheets **113**, 2841 (2012).

[32] G. Gürdal and F. G. Kondev, Nucl. Data Sheets **113**, 1315 (2012).
[33] S. Galanopoulos, P. Demetriou, M. Kokkoris, S. Harissopulos, R. Kunz, M. Fey, J. W. Hammer, Gy. Gyürky, Zs. Fülöp, E. Somorjai, and S. Goriely, Phys. Rev. C **67**, 015801 (2003).
[34] A. Sauerwein, J. Endres, L. Netterdon, A. Zilges, V. Foteinou, G. Provatas, T. Konstantinopoulos, M. Axiotis, S. F. Ashley, S. Harissopulos, and T. Rauscher, Phys. Rev. C **86**, 035802 (2012).
[35] S. Harissopulos, A. Spyrou, A. Lagoyannis, M. Axiotis, P. Demetriou, J. W. Hammer, R. Kunz, and H.-W. Becker, Phys. Rev. C **87**, 025806 (2013).
[36] J. Mayer, S. Goriely, L. Netterdon, S. Peru, P. Scholz, R. Schwengner, and A. Zilges, Phys. Rev. C **93**, 045809 (2016).
[37] L. Netterdon, A. Endres, S. Goriely, J. Mayer, P. Scholz, M. Spieker, and A. Zilges, Phys. Lett. B **744**, 358 (2015).
[38] F. Heim, J. Mayer, M. Müller, P. Scholz, M. Weinert, and A. Zilges, Nucl. Instrum. Methods Phys. Res., Sect. A **966**, 163854 (2020).
[39] F. Heim, P. Scholz, J. Mayer, M. Müller, and A. Zilges, Phys. Rev. C **101**, 035807 (2020).
[40] J. Ziegler, J. Biersack, and M. Ziegler, *SRIM - The Stopping and Range of Ions in Matter*, http://www.srim.org.
[41] Huo Junde, Huo Su, and Yang Dong, Nucl. Data Sheets **112**, 1513 (2011).
[42] E. Browne and J. K. Tuli, Nucl. Data Sheets **111**, 1093 (2010).
[43] P. Scholz, M. Guttormsen, F. Heim, A. C. Larsen, J. Mayer, D. Savran, M. Spieker, G. M. Tveten, A. V. Voinov, J. Wilhelmy, F. Zeiser, and A. Zilges, Phys. Rev. C **101**, 045806 (2020).
[44] S. Goriely, S. Hilaire, and A. J. Koning, Phys. Rev. C **78**, 064307 (2008).
[45] M. Martini, S. Péru, S. Hilaire, S. Goriely, and F. Lechaftois, Phys. Rev. C **94**, 014304 (2016).
[46] S. Goriely, S. Hilaire, S. Péru, and K. Sieja, Phys. Rev. C **98**, 014327 (2018).
[47] C. H. Johnson, C. C. Trail, and A. Galonsky, Phys. Rev. **136**, B1719 (1964).
[48] A. B. Smith, P. T. Guenther, and J. F. Whalen, Nucl. Phys. A **415**, 1 (1984).
[49] A. Koning and J. Delaroche, Nucl. Phys. A **713**, 231 (2003).
[50] A. Schiller, L. Bergholt, M. Guttormsen, E. Melby, J. Rekstad, and S. Siem, Nucl. Instrum. Methods Phys. Res., Sect. A **447**, 498 (2000).
[51] A. Koning, S. Hilaire, and S. Goriely, Nucl. Phys. A **810**, 13 (2008).
[52] S. Hilaire and S. Goriely, Nucl. Phys. A **779**, 63 (2006).
[53] W. Dilg, W. Schantl, H. Vonach, and M. Uhl, Nucl. Phys. A **217**, 269 (1973).
[54] A. Gilbert and A. G. W. Cameron, Can. J. Phys. **43**, 1446 (1965).
[55] A. Voinov, S. M. Grimes, C. R. Brune, M. Guttormsen, A. C. Larsen, T. N. Massey, A. Schiller, and S. Siem, Phys. Rev. C **81**, 024319 (2010).
[56] A. C. Larsen *et al.*, Phys. Rev. C **87**, 014319 (2013).
[57] S. Goriely and E. Khan, Nucl. Phys. A **706**, 217 (2002).
[58] I. Daoutidis and S. Goriely, Phys. Rev. C **86**, 034328 (2012).
[59] S. Goriely, E. Khan, and M. Samyn, Nucl. Phys. A **739**, 331 (2004).
[60] A. Voinov, E. Algin, U. Agvaanluvsan, T. Belgya, R. Chankova, M. Guttormsen, G. E. Mitchell, J. Rekstad, A. Schiller, and S. Siem, Phys. Rev. Lett. **93**, 142504 (2004).
[61] M. Guttormsen *et al.*, Phys. Rev. C **71**, 044307 (2005).
[62] A. Leprêtre, H. Beil, R. Bergère, P. Carlos, A. De Miniac, A. Veyssière, and K. Kernbach, Nucl. Phys. A **219**, 39 (1974).